ISSN 0915-633X

NATIONAL INSTITUTE FOR FUSION SCIENCE

Shafranov Shift in Low-Aspect-Ratio Heliotron/Torsatron CHS

H. Yamada, K. Ida, H. Iguchi, S. Morita
O. Kaneko, H. Arimoto, M. Hosokawa, H. Idei
S. Kubo, K. Matsuoka, K. Nishimura, S. Okamura
Y. Takeiri, Y. Takita, C. Takahashi, K. Hanatani
H. C. Howe, S. P. Hirshman and D. K. Lee

(Received – Aug. 29, 1991)

NIFS-110 Sep. 1991

RESEARCH REPORT
NIFS Series

NAGOYA, JAPAN

SHAFRANOV SHIFT IN LOW-ASPECT-RATIO HELIOTRON/TORSATRON CHS

H.YAMADA, K. IDA, H.IGUCHI, K. HANATANI*, S.MORITA, O.KANEKO, H.C.HOWE†, S.P.HIRSHMAN†, D.K.LEE†, H.ARIMOTO, M.HOSOKAWA, H.IDEI, S.KUBO, K.MATSUOKA, K.NISHIMURA, S.OKAMURA, Y.TAKEIRI, Y.TAKITA, C.TAKAHASHI

National Institute for Fusion Science, Nagoya 464-01, Japan

**Plasma Physics Laboratory, Kyoto University, Uji 611, Japan*

†Oak Ridge National Laboratory, Oak Ridge, TN37831, USA

The MHD equilibrium properties of neutral-beam-heated plasmas have been experimentally investigated in the Compact Helical System (CHS), a low-aspect-ratio ($A_p \sim 5$) heliotron/torsatron. This configuration is characterized by a strong breaking of helical symmetry. The radial profiles measured by various diagnostics have shown significant Shafranov shift due to plasma pressure. The deviation of the magnetic axis from its vacuum position has reached 50% of the minor radius. When the three-dimensional equilibrium code VMEC is used to reconstruct the equilibrium from the experimental data, the result is in good agreement with the experimentally observed Shafranov shift as well as the diamagnetic pressure in plasmas with $\langle\beta\rangle \leq 1.2\%$ and $\beta_0 \leq 3.3\%$. This β value corresponds to half of the conventional equilibrium β limit defined by the Shafranov shift reaching a value of half the minor radius. Although tangential neutral beam injection has caused pressure anisotropies $p_{//}/p_{\perp} \leq 3$, the description of the equilibrium assuming isotropic pressure is consistent with the experiment.

Keywords: Shafranov shift, Equilibrium β limit, CHS, VMEC, Low aspect ratio

1.INTRODUCTION

Magnetohydrodynamic (MHD) equilibria of toroidal plasmas have been studied for a variety of magnetic configurations since the beginning of magnetic fusion research (see Ref.[1] as a pioneering work). For axisymmetric (two-dimensional (2-D)) configurations, e.g. the tokamak, the theory is well developed and its applications to experiments have been quite successful. MHD theory has been used for precise control of the position of the plasma column and realization of the divertor configuration. Description of the tokamak equilibrium by the ideal MHD model has been experimentally proven to agree with the theoretical equilibrium limit [2]. The equilibrium theory has been also extended to systems with pressure anisotropy due to fast ions or energetic electrons, and self-consistent solutions have been successfully derived [3-5].

Although studies of asymmetric systems, e.g. the stellarator, have also progressed [6], their applicability to experiments still seems to be limited due to the complexity associated with three-dimensional (3-D) geometry. However, recent rapid advances in numerical computation provide a systematic picture of 3-D equilibria with finite β (the ratio of the gas kinetic pressure to the magnetic field pressure). Although the existence of equilibrium solutions is not clear in the strict mathematical sense for a toroidal helical system [7], most all models presume the existence of closed, nested magnetic surfaces. If the ergodic spatial scale of magnetic field lines is much smaller than the Larmor radius, this approximation is assumed to be applicable to experiments. To get a 2-D equation for the toroidally averaged poloidal flux function, the approximation of large aspect ratio, called the stellarator expansion [8] or the averaging method [9,10] has also been used. While the equilibrium theory for axisymmetric systems has been confirmed in the framework of MHD, that for asymmetric systems has been advanced on the basis of these approximations. Therefore, comparison of the theoretical model with experiments is of much importance to resolve the limitations of the model.

The magnetic axis shift due to plasma pressure has been observed in Wendelstein

VII-A and the result has been compared with the linear analytic theory for a few examples [11]. Also, in Wendelstein VII-AS, which is designed to reduce the Pfirsh-Schlüter current on the basis of the ideal MHD theory, the observed magnetic axis shift is smaller than that in a conventional stellarator, as expected [12], but the accuracy of this data is not sufficient to get a precise comparison with the theory.

As seen in a series of Wendelstein and Heliotron devices (see Ref. [13] as a review), toroidal helical systems have traditionally had large aspect ratio, with therefore only a small breaking of helical symmetry. Recently, MHD characteristics in low-aspect-ratio heliotron/torsatron have been investigated theoretically, and various critical physics issues have been presented for experimental study [14,15]. The Shafranov shift Δ is estimated for the low β case from the stellarator expansion as $\Delta = \beta_0 A_p a / \iota(a)^2$, where β_0, A_p, a, and ι are the central β, the aspect ratio, the minor radius, and the rotational transform, respectively. Since ι is proportional to A_p in general, Δ is enhanced in a low-aspect-ratio configuration, where toroidicity is enhanced. A large Shafranov shift results in efficient generation of a magnetic well, which tends to stabilize the interchange instability, but causes a low equilibrium β limit. Also, large distortion of the magnetic-surface structure might cause deterioration of confinement. The description of finite-β equilibria is a prerequisite for MHD stability analysis as well as various transport analyses.

In order to verify the validity of the available MHD equilibrium model, it is desirable to investigate a low-aspect-ratio configuration with strong breaking of symmetry. We compare the experimental results for MHD equilibria with a theoretical model in a heliotron/torsatron configuration with an aspect ratio as low as 5, which is uniquely low for a toroidal helical system.

2. EXPERIMENT IN CHS

The compact helical system (CHS) is a heliotron/torsatron device with poloidal mode number l=2 and toroidal mode number m=8 designed to resolve various physics

issues of the stellarator/heliotron/torsatron concept in a low-aspect-ratio regime[16,17]. The major radius of the vacuum vessel and the helical coils R is 1m and the plasma minor radius a is up to 0.21m, which leads to a plasma aspect ratio A_p of 5. The major radius of the vacuum magnetic axis R_{ax} can be controlled by a vertical magnetic field. Since a variety of plasma production techniques (28GHz and 53GHz ECRF, 7.5MHz and 13MHz ICRF) are available in the CHS, the operational toroidal field has much flexibility. An auxiliary neutral beam (NB) with power of up to 1.1MW and energy of up to 40keV was injected tangentially into target plasmas to sustain quasi-steady-state plasmas for up to 1s. Since no active control of the vertical field was applied during the heating phase, the spontaneous vertical field due to Pfirsh-Schlüter currents shifted the plasma column outward for free-boundary conditions.

Although the helical coils prevent wide access for diagnostics in conventional stellarator/heliotron/torsatron devices, the low aspect ratio of the CHS provides large ports for profile measurements. The density and temperature of electrons were measured by a spatially resolved Thomson scattering system, and the ion temperature was obtained by charge-exchange recombination spectroscopy (CXRS) with 7.5-mm spatial resolution [18,19]. Figure 1(a) shows the experimental setup of the CXRS system and the vacuum magnetic surfaces with R_{ax} = 0.92 m for the vertically elongated cross-section. The view of the CXRS diagnostics covers almost the entire plasma. Since the density profile has been, in general, rather flattened or slightly hollow in the central region of CHS plasmas, the pressure profile is expected to follow the ion temperature profile. Therefore, the peak of the ion temperature profile should correspond with the position of the magnetic axis. Figure 1(b) shows the measured plasma profiles with n_e=1.5×10^{19}/m^3, the absorbed beam power P_{abs} ~400kW, and R_{ax} = 0.92m. The normalized minor radius ρ is derived from the projection onto the one-dimensional (1-D) geometry using the vacuum flux surface shown in Fig.1(a). The solid line is the least-squares fitting of the ion temperature profile, $(T_i(0)\text{-}T_i(1))(1\text{-}\rho^{\alpha})^{\beta} + T_i(1)$, where α and β are the fitting variables. Clearly, there is an outward shift of the profile, i.e., the

Shafranov shift. The peak in the ion temperature was located 3cm outside the vacuum R_{ax}. The electron temperature and density profiles also indicated outward shifts, although accurately estimating the position of the peak was difficult because of the limitation ($R > 0.92$ m) of the scope of the Thomson scattering system. The Shafranov shift has also been observed in the soft X-ray emission profile, which is line integrated. In this work, we place emphasis on the results from the CXRS, since we can estimate the change of equilibrium most accurately from it among available diagnostics. Diamagnetic measurement of the integrated perpendicular energy is also discussed. The effect of three-dimensionality on diamagnetic flux is small except for the paramagnetic flux due to the net current flowing along the field line [20].

3. ANALYSIS OF EQUILIBRIUM

In this section we describe the procedure to construct the 3-D equilibrium from kinetic data obtained in the experiment [21]. The pressure profile is calculated with the 1-D profile analysis code PROCTR-MOD [22] from the experimental profile measurements ($T_e(R)$,$T_i(R)$,$n_e(R)$). The relationship between the real-space experimental coordinates and the plasma flux surface coordinate ρ is derived from an inverse geometry representation. The calculated pressure profile is used to recalculate the magnetic configuration by the 3-D free boundary equilibrium code VMEC [23].

Figure 2 (a) shows the magnetic surfaces of the finite-β equilibrium for the discharge described in Section 2, which was obtained by taking account of the thermal pressure, i.e., $p_{th} = n_eT_e+(n_i+n_{imp})T_i$. The calculated shift of the magnetic axis was only 1.1 cm, which is much smaller than the experimental observation. There remains discrepancy between the experimental T_i profile and the equilibrium pressure surfaces(see Fig.2(b)). The β value based on kinetic data was 0.18%, while $<\beta_{dia}>$ from diamagnetic measurement was 0.26%, where the brackets <> indicate a volume-averaged value. These discrepancies suggest that the equilibrium obtained by considering

only thermal pressure is not self-consistent. The impurity concentration as measured with a VUV spectrometer suggests that Z_{eff} was dominated by carbon and oxygen ions, and that the value was Z_{eff} = 2~3.5 in the analyzed discharges. Throughout this work, the main impurity is assumed to be oxygen, and Z_{eff} is set equal to 2.0 and constant in space. Although this assumption leads to error in estimating dilution, its effect on thermal pressure is within several percent, which makes a negligible difference in the experimental error. Impurity concentration also affects the power deposition of NB, however, this error discrepancy is even smaller.

In the example discharge, the slowing-down time of fast ions was roughly 4 ms while the global confinement time was 1.5 ms. This means that the unthermalized pressure due to fast ions makes a major contribution to the MHD equilibrium. From this example, it is clear that the beam makes a significant contribution to the equilibrium of NB-heated plasmas in the CHS. Therefore, a precise estimate of the beam pressure is a prerequisite for the accurate calculation of MHD equilibrium.

Low aspect ratio causes a large deviation of particle orbits from magnetic surfaces, as well as a large loss cone. In the case of transit particles with an energy of 40keV, the deviation reaches half of the minor radius at 1T operation. This complicates evaluation of the beam pressure. The power deposition on each magnetic surface is affected by this orbit deviation; in particular, orbit loss and charge-exchange loss. The precise estimate of these effects requires a Monte-Carlo simulation which can deal with the 3-D geometry including the vacuum region outside the plasma. Alternative analytical formulas [24] in the equivalent averaged axisymmetric geometry, which are employed in the PROCTR-MOD code, facilitate the iteration scheme of reconstructing equilibria[25]. We have incorporated a semi-empirical model of the 3-D orbit effect into the beam deposition calculation in PROCTR-MOD. This semi-empirical model is based on a number of parameter runs of the 3-D Monte-Carlo particle code HELIOS [26]. The behavior of fast ion orbits in the CHS will be discussed in detail elsewhere.

Since the current carried by the fast ions is negligibly small compared with the plasma secondary current, we can omit the effect of the deviation of its orbit from the

magnetic surface. This means that it is sufficient to consider only the flux-surface-averaged pressure. The large parallel velocity and small pitch angle due to tangential injection result in significant anisotropy of the beam pressure. The effect of pressure on the equilibrium is primarily attributed to the vertical field generated by the Pfirsh-Schlüter current. When we write a pressure tensor as $\mathbf{P} = p_{\perp}\mathbf{I} + (p_{//} - p_{\perp})\,\mathbf{nn}$, where $\mathbf{I}$, $\mathbf{n}$, $p_{//}$, and $p_{\perp}$ are the unit tensor, the unit vector along the magnetic field, the parallel pressure, and the perpendicular pressure, respectively, the Pfirsh-Schlüter current is proportional to $\nabla(p_{//} + p_{\perp})$ [27]. In this work, therefore, we approximate the scalar pressure p by $p_{th} + (p^b{}_{//} + p^b{}_{\perp})/2$, where p^b denotes the beam pressure. The equilibrium beta β_{eq} is defined by this pressure, and the perpendicular beta $\beta_{\perp}$ which corresponds to the diamagnetic beta β_{dia} is calculated from $p_{th} + p^b{}_{\perp}$.

Iteration between PROCTR-MOD and VMEC, including the contribution of beam pressure, has been done until the geometry and plasma profiles converge. Figure 3(a) shows the final equilibrium indicating the 3.3cm magnetic axis shift from its vacuum position. The consequent T_i profile shows good agreement with the 1-D fitting (Fig. 3(b)). The perpendicular pressure estimated from the reconstructed equilibrium is $<\beta_{\perp}>=0.29\pm0.2\%$, which also agrees well with the experiment. To achieve these satisfactory agreements, it was necessary to take account of the fast ion orbit effects in the beam pressure calculation such as flattening of the deposition profile in the core region. This agreement indicates that a self-consistent equilibrium is obtained and that the present procedure is successful in describing MHD equilibrium of low-aspect-ratio CHS plasmas.

Figure 4 shows the resultant pressure profile. Although the beam pressure is dominant ($2p_{th}/(p^b{}_{//} + p^b{}_{\perp}) \sim 0.5$) and the anisotropy $p_{//}/p_{\perp}$ reaches 2.5, the present analysis gives an equilibrium consistent with the experimental observation. Even when the birth profile of fast ions is peaked, the pressure profile becomes flattened or hollow in the core region due to the orbit effect.

4.RESULTS

Profile analysis has been conducted for co- and counter- NB heated plasmas with B_t = 0.45 ~ 1.5 T, n_e = 0.8 ~ 5.5 × 10^{19}m^{-3}, R_{ax} = 0.89 ~ 1.02m, $<\beta_{eq}>$ = 0.15 ~ 1.2 %. The beam pressure ratio $<p^b> / 2<p_{th}>$ was in the range of 0.2 ~ 2.0. The usual equilibrium limit corresponds to the configuration where the Shafranov shift Δ reaches half the minor radius. At this point, the distortion of magnetic surface structure becomes quite large. It should be noted that the magnetic axis shift giving this limit, Δ_{limit}, does not correspond to $a/2$, since the vacuum magnetic axis is originally shifted depending on the magnetic configuration. For example, the position of the vacuum magnetic axis in the case of R_{ax} = 0.90 m and 1.02 m is shifted 2.1 cm inward and 4.6 cm outward, respectively, from the center of the boundary surface on the vertically elongated cross section. In the most shifted case (R_{ax} = 0.90 m), the experimentally obtained magnetic axis shift Δ_{exp} was around 60% of Δ_{limit} and close to half the minor radius. In terms of $<\beta_{eq}>$, the highest experimental value has reached roughly 50% of the critical value.

Figure 5 shows a comparison of the magnetic axis shift derived from the T_i profile with the theoretical prediction which is applicable in the linear response regime, i.e. $\Delta \propto \beta$. The data are normalized by Δ_{limit}. The shift of the magnetic surface relative to the boundary surface is given by [6]

$$\Delta(r) = -\int_0^a \frac{2R(\bar{p}(r) - p(r))}{\mu_0 B_0^2 \iota^2 r} \mathrm{d}r, \qquad (1)$$

where

$$\bar{p} = \frac{2}{r^2}\int_0^r p(r) r \, \mathrm{d}r \quad .$$

When the experimental shift is less than one third of Δ_{limit}, the experimental results agree with the linear theory. Within this range, Eq.(1) is found to be applicable even for the CHS where the aspect ratio is as low as 5. Above this range, however, the plasma

does not respond linearly and the rate of increase in the shift is much reduced with increasing β. The numerical studies have shown a similar trend for various torsatron configuration [15]. If we eliminate the beam pressure, the theoretical prediction, Eq.(1), gives a systematically smaller value than that from the experiment. This trend indicates the importance of beam pressure in reconstructing the equilibria mentioned in Section 3.

Using the scheme described in Section 3 for reconstructing equilibria from profile data sets, we can examine the applicability of the 3-D numerical calculations. For magnetic axis shift, we can see a remarkable correlation between the experiment and the calculation over a wide range of plasma parameters within the accuracy of the present methods (see Fig.6). The reconstructed equilibrium has been also verified by the comparison of integrated perpendicular pressure. Figure 7 shows the ratio of $<\beta_\perp>$ to $<\beta_{dia}>$ as a function of electron density. Taking the beam pressure into account, we can see a close agreement between the measured and calculated values. The variation observed at lower density, when $<\beta_{dia}>$ is smaller, is due to (1) the signal-to-noise level in the magnetic diagnostics and (2) the beam-driven current, which becomes larger with decreasing the density and produces paramagnetic flux. As the density decreases, the slowing down time of fast ions becomes longer; thus the beam pressure contributes proportionally more in the lower density case. When the beam pressure is omitted from the calculation, $<\beta_\perp> / <\beta_{dia}>$ is systematically below 1 and a larger discrepancy is observed at lower density.

As mentioned in Section 3, the present group of discharges were characterized by anisotropic pressures. The anisotropy $<p_{//}> / <p_\perp>$ has been in the range between 1.1 and 2.5. Equilibria with pressure anisotropy have been studied theoretically by many researchers [3-5,28,29]. It has been theoretically pointed out for tokamak plasmas that the magnetic axis shift in the presence of pressure anisotropy is different from that in the isotropic case [28]. However, any trend correlated with anisotropy has not been observed experimentally in the equilibria considered here.

5.DISCUSSION

We have presented the 3-D experimental analysis of MHD equilibria which has been shown to be self-consistent for plasmas with aspect ratio as low as 5 by comparison with the 3-D numerical computation of the magnetic axis shift and diamagnetic flux. However, the investigated plasmas certainly lie below the equilibrium β limit. Figure 8 shows an operational diagram of $<\beta>$ as a function of vacuum magnetic axis position. The group of discharges presented in this work were distributed in the hatched area. When we approximated the pressure profile by $p(\rho) = p_0 (1 - \rho^2)^{\alpha}$, the value of α was within the range of 1.5 ~ 2.5 for every discharge. Two kinds of equilibrium β limits calculated for the case of $\alpha = 2$ are illustrated, one of which is the conventional limit used in Section 4 and the other is the limit of availability of an equilibrium solution in the present 3-D numerical analysis. These limits are rather different. The broken line in Fig.8 is the range we have realized in CHS, but a complete profile data set has not been available. For those plasmas that fall within these limits, there seemed to be consistency with the extrapolation of the present work.

Although whether a numerical solution is obtained depends to some extent on the numerical scheme and mesh resolution, the reason for disappearance of the solution in the high-β regime may be physically attributed to the appearance of a separatrix in the closed magnetic surfaces or splitting of the magnetic axis. Alternatively, the conventional equilibrium β limit comes from a naive conclusion that the distortion of magnetic flux surfaces is intolerable. Therefore, this limit is convenient but may not have a clear physical justification [30]. Also, magnetic surface breaking may occur in 3-D finite-β plasmas, which reduces β [31,32]. A picture of the equilibrium-β limit in asymmetric plasmas has not been clarified either theoretically or experimentally yet. Demonstration over the conventional β limit and the examination of the 3-D numerical analysis close to the limit wait for near-future experiments.

In the CHS, the measured equilibrium β limit is lower than the MHD stability limit

under the free boundary condition without vertical field control during heating. However, fluctuations associated with the resistive interchange mode have been observed. The pressure anisotropy is supposed to have only a small effect on equilibrium, which has been supported by this work, but a significant effect on MHD stability [29]. Therefore NB-heated plasmas in the CHS requires further analysis to access the stability boundaries in the presence of pressure anisotropy.

ACKNOWLEDGEMENTS

We acknowledge with appreciation the contribution of Dr.R.N.Morris and Prof. T.Amano to numerical code handling; and Dr.M.Murakami to smoothing the way for collaboration. We gratefully acknowledge useful discussions with Dr.S.Yoshikawa and Dr.Z.Yoshida and continuing encouragement of Dr.A.Iiyoshi.

REFERENCES

[1] GRAD,H., RUBIN,H., in *Proceedings of the Second United Nations Conference on the Peaceful Uses of Atomic Energy* (NATO, Geneva, 1958), Vol.31, p.190.

[2] NAVRATIL,G.A., GROSS,R.A., MAUEL,M.E., SABBAGH,S.A., BELL,M.G.,et al., to appear in *Plasma Physics and Controlled Nuclear Fusion, 1990*, Washington (IAEA, Vienna,1991).

[3] GRAD, H., in *Magneto-Fluid and Plasma Dynamics, Symposia in Applied Mathematics* (American Mathematical Society, 1967), Vol.18, p.162.

[4] COOPER,W.A., BATEMAN,G., NELSON,D.B., KAMMASH,T., Nucl. Fusion **20** (1980) 985.

[5] YOSHIDA,Z., Phys. Fluids B **1** (1989) 1702.

[6] PUSTOVITOV, V.D., SHAFRANOV, V.D., in *Reviews of Plasma Physics*

(Consultant Bureau, New York 1990), Vol.15, p.163 .

[7] GRAD,H., Phys. Fluids **10** (1967) 137.

[8] GREEN, J.M., JOHNSON, J.L., Phys. Fluids **4** (1961) 875.

[9] KOVRIZHNYKH, L.M., SHCHEPETOV,S.V., Fiz. Plazmy **6** (1980) 976.

[10] STRAUSS,H.R., Plasma Phys. Controlled Fusion **22** (1980) 733.

[11] DORST,D., ELSNER,A., GRIEGER,G., Plasma Phys. Controlled Fusion **26** 1A (1984) 183.

[12] WELLER,A., BRAKEL,R., BURHENN,R., HACKER,H., LAZAROS,A., in *Controlled Fusion and Plasma Physics* (Proc. 17th Europ. Conf. Amsterdam, 1990), Vol.19B, Part II (1990) 479.

[13] CARRERAS,B.A., GRIEGER,G., HARRIS,J.H., JOHNSON,J.L., LYON,J.F., et al., Nucl. Fusion **28** (1988) 1613.

[14] CARRERAS, B.A., Comments Plasma Phys. Controlled Fusion **11** (1987) 139.

[15] CARRERAS,B.A., DOMINGUEZ,N., GARCIA,L., LYNCH,V.E., LYON,J.F., et al., Nucl. Fusion **28** (1988) 1195.

[16] MATSUOKA,K., KUBO,S., HOSOKAWA,M., TAKITA,Y., OKAMURA,S., et al., in *Plasma Physics and Controlled Nuclear Fusion, 1988* (Proc. 12th Int. Conf. Nice, 1988) , Vol. 2, IAEA, Vienna (1989) 411.

[17] NISHIMURA,K, MATSUOKA,K., FUJIWARA,M., YAMAZAKI,K., TODOROKI, J., et al., Fusion Technol. **17** (86) 1990.

[18] IDA, K., HIDEKUMA, S., Rev. Sci. Instrum. **60** (1989) 876.

[19] IDA, K., YAMADA, H., IGUCHI, H., HIDEKUMA, H., SANUKI, H., et al., Phys. Fluids B **3** (1991) 515.

[20] A toroidal net current of up to 7 kA has been observed in the discharges of the present database. It is supposed to be due to beam driven (Ohkawa) current and bootstrap current. (see KANEKO,O., KUBO,S., NISHIMURA,K., SHOJI,T., HOSOKAWA,M., et al., to appear in *Plasma Physics and Controlled Nuclear Fusion, 1990*, (Proc. 13th Int. Conf. Washington, 1990) , IAEA, Vienna (1991)). The effect of the toroidal current on equilibrium is considered with

estimate of current profile from the tokamak formulas, however, it is quite small.

[21] HOWE,H.C., HORTON,L.D., CRUME,E.C., et al., in *Controlled Fusion and Plasma Physics* (Proc. 16th Europ. Conf. Venice, 1989), Vol.13B, Part II (1989) 683.

[22] HIRSHMAN, S.P., Comput. Phys. Commun. **43** (1986) 143.

[23] YAMADA, H., IDA,K., IGUCHI,H., HOWE,H.C., KUBO,S., et al., in *Controlled Fusion and Plasma Physics* (Proc. 18th Europ. Conf. Berlin, 1991), Part II (1991) 137.

[24] ROME,J.A., CALLEN,J.D., CLARKE,J.F., Nucl. Fusion **14** (1974) 141.

[25] The analytic formulas in PROCTR-MOD give a good approximation for the birth profile of fast ion and shine-through loss in the case of tangential injection. This fact has been verified by comparing these formulas with results from HELIOS in the CHS geometry.

[26] FOWLER,R.H., MORRIS,R.N., ROME,J.A., HANATANI,K., Nucl. Fusion **30** (1990) 997.

[27] HITCHON,W.N.G., Nucl. Fusion **23** (1983) 383.

[28] SESTERO,A., TARONI,A., Nucl. Fusion **16** (1976) 164.

[29] BUCKLE,K.A., HITCHON,W.N.G., SHOHET, J.L., Nucl. Fusion **25** (1985) 247.

[30] In some specific cases with parabolic pressure profile, this limit corresponds to $\varepsilon \beta_p = 1$ in tokamak configuration, where ε is $1/A_p$ and β_p is the poloidal beta.

[31] HAYASHI,T., SATO,T., TAKEI,A., Phys. Fluids B **2** (1990) 329.

[32] REIMAN, A.H., BOOZER, A.H., Phys. Fluids **27** (1984) 2446.

Figure captions

Figure 1 *(a) Cross section of the vacuum magnetic flux surfaces (R_{ax}=0.92m) at the location of the charge exchange recombination spectroscopy (CXRS) diagnostic which gives the point data along Z=0. (b) Profiles of ion temperature measured by CXRS, and electron temperature and density measured by Thomson scattering during a sample discharge. Minor radius is normalized using the vacuum flux surfaces shown in Fig.1 (a). The minor radius of the data inside the magnetic axis is set to have a negative sign for convenience in plotting. The 1-D fitting curve of T_i profile has a function ; $T_i(\rho) = (T_i(0)-T_i(1))(1-\rho^{\alpha})^{\beta}+T_i(1)$.*

Figure 2 *(a) Cross section of the magnetic flux surfaces of the finite-β equilibrium considering only thermal pressure (solid lines) and those of the vacuum magnetic field (dot-dash lines). (b)Ion temperature measured by CXRS and the 1-D fitting curve.*

Figure 3 *(a) Cross section of the magnetic flux surfaces of the finite-β equilibrium which results from repeated iteration of calculations in PROCTR-MOD and VMEC considering both thermal pressure and fast-ion pressure from beam (solid lines) and those of the vacuum magnetic field (dot-dash lines). (b)Ion temperature measured by CXRS and the 1-D fitting curve.*

Figure 4 *Pressure profile of a sample discharge, which is consequently obtained from the present 3-D numerical analysis.*

Figure 5 *Comparison of the magnetic axis shift from the position in the vacuum*

magnetic field estimated from the theory applicable to the linear response regime with the experimental observation. The value of the shift is normalized by the critical value for each magnetic configuration. The case taking account of beam pressure is shown by closed circles and the case omitting it by open circles.

Figure 6 *Comparison of the magnetic axis shift estimated from the 3-D numerical analysis Δ_{cal} with the experimental observation Δ_{exp} on the vertically elongated cross section. The data are normalized by the radius on the shorter axis; a_s*

Figure 7 *The ratio of the volume-averaged perpendicular pressure estimated from the 3-D numerical analysis to the experimental value measured by the diamagnetic diagnositics as a function of the line-averaged density.The case taking account of beam pressure is shown by closed circles and the case omitting it by open circles.*

Figure 8 *Diagram of equilibrium β limit in CHS. The β limits are calculated for the parabolic pressure profile; $p(r) = p_0 (1-\rho^2)^{\alpha}$ and $\alpha = 2$. The error bar indicates the pressure profile effect. The upper case $\alpha = 1.5$ and the lower case $\alpha = 2.5$.*

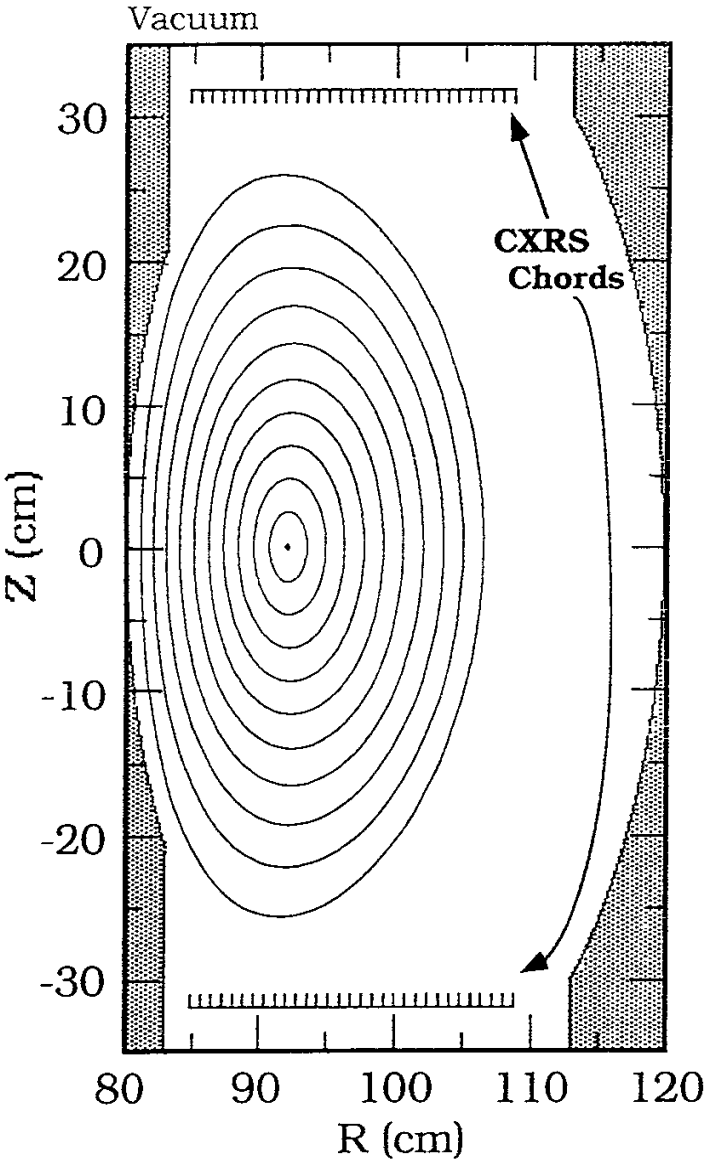

Figure 1 (a)

"Shafranov Shift in Low-Aspect-Ratio Heliotron/Torsatron CHS" by H.Yamada et al., *National Institute for Fusion Science, Nagoya 464-01, JAPAN*

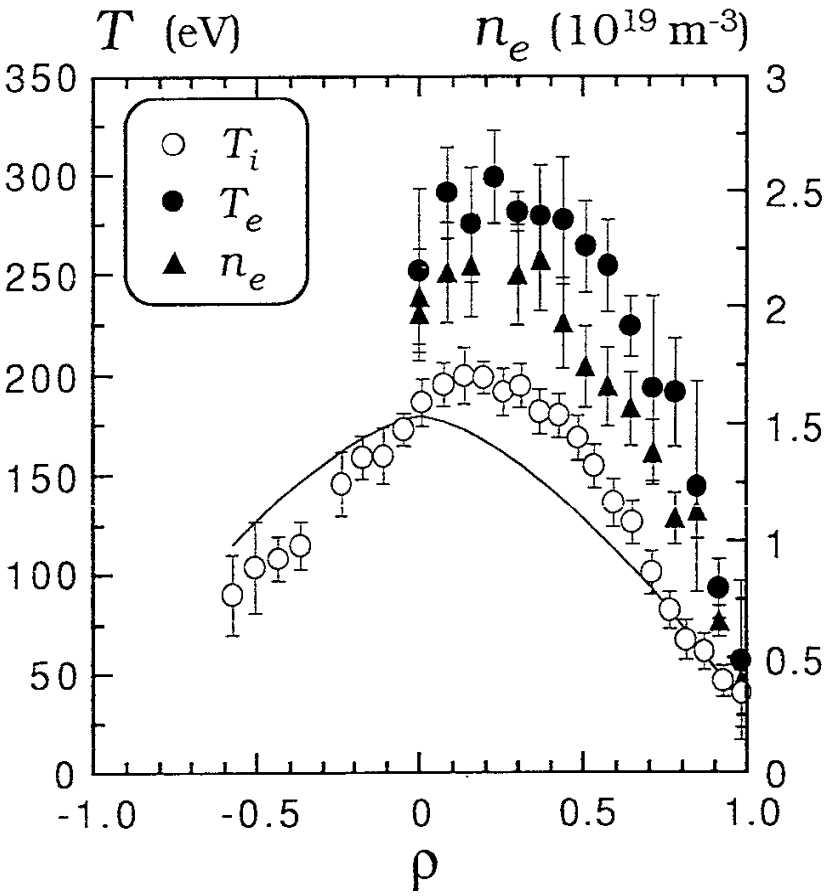

Figure 1 (b)

"Shafranov Shift in Low-Aspect-Ratio Heliotron/Torsatron CHS" by H.Yamada et al., *National Institute for Fusion Science, Nagoya 464-01, JAPAN*

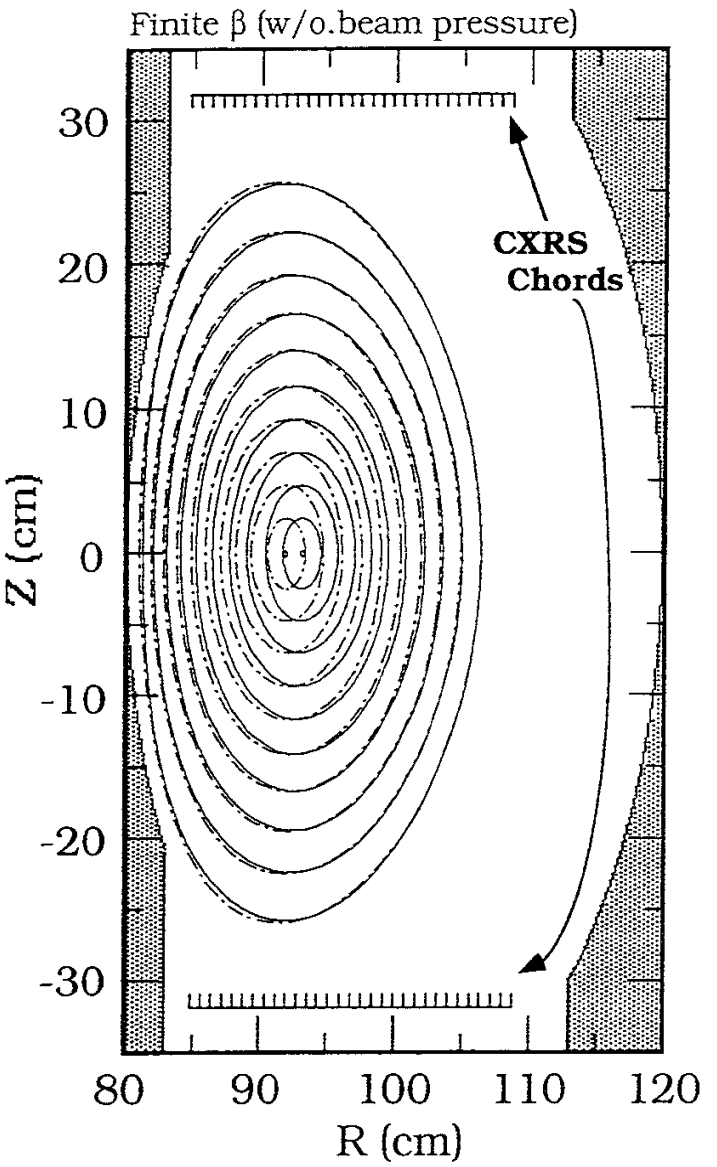

Figure 2 (a)

"Shafranov Shift in Low-Aspect-Ratio Heliotron/Torsatron CHS" by H.Yamada et al., *National Institute for Fusion Science, Nagoya 464-01, JAPAN*

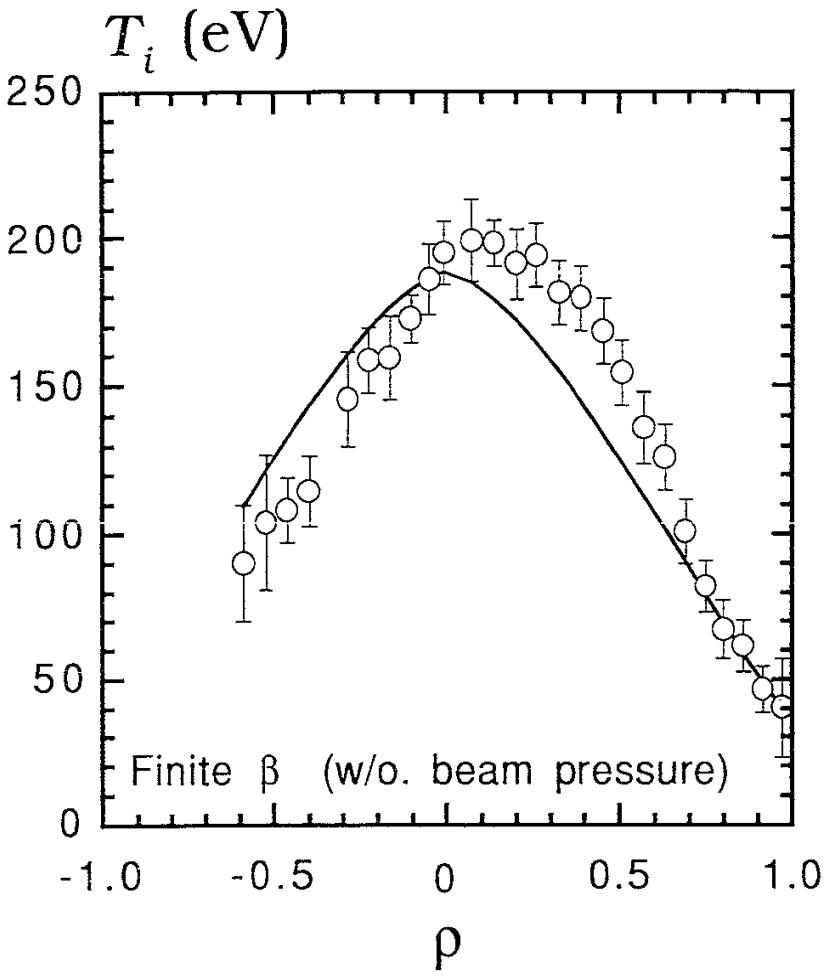

Figure 2 (b)

"Shafranov Shift in Low-Aspect-Ratio Heliotron/Torsatron CHS" by H.Yamada et al., *National Institute for Fusion Science, Nagoya 464-01, JAPAN*

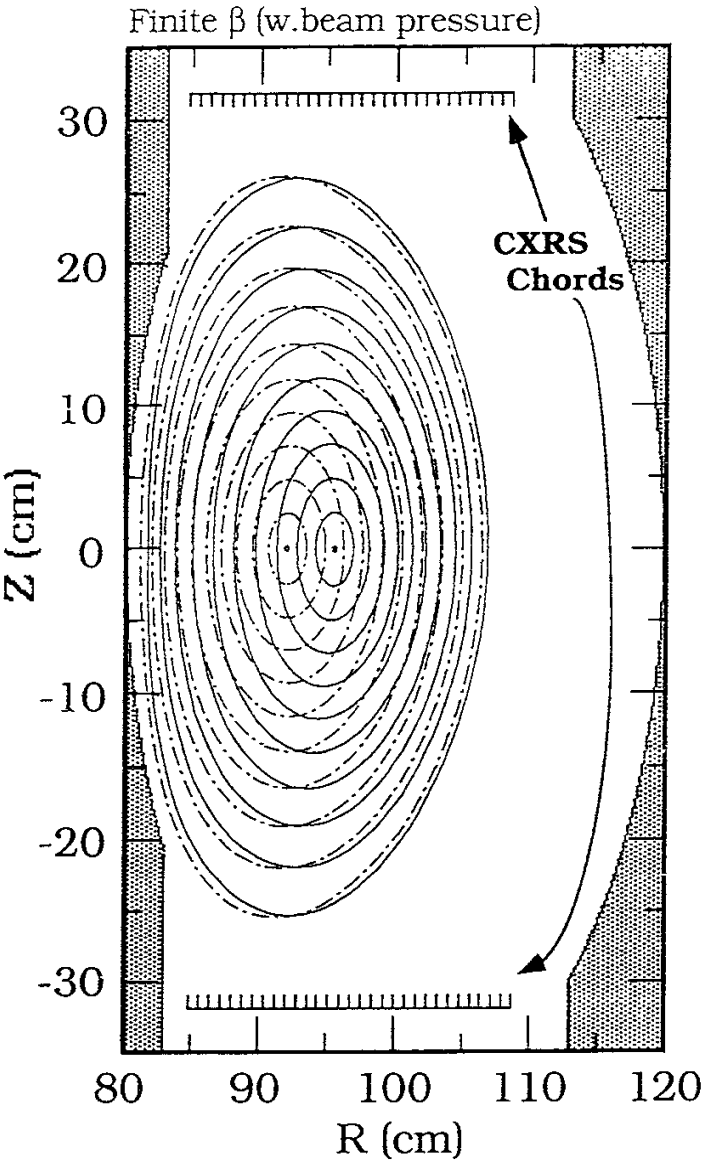

Figure 3 (a)

"Shafranov Shift in Low-Aspect-Ratio Heliotron/Torsatron CHS" by H.Yamada et al., *National Institute for Fusion Science, Nagoya 464-01, JAPAN*

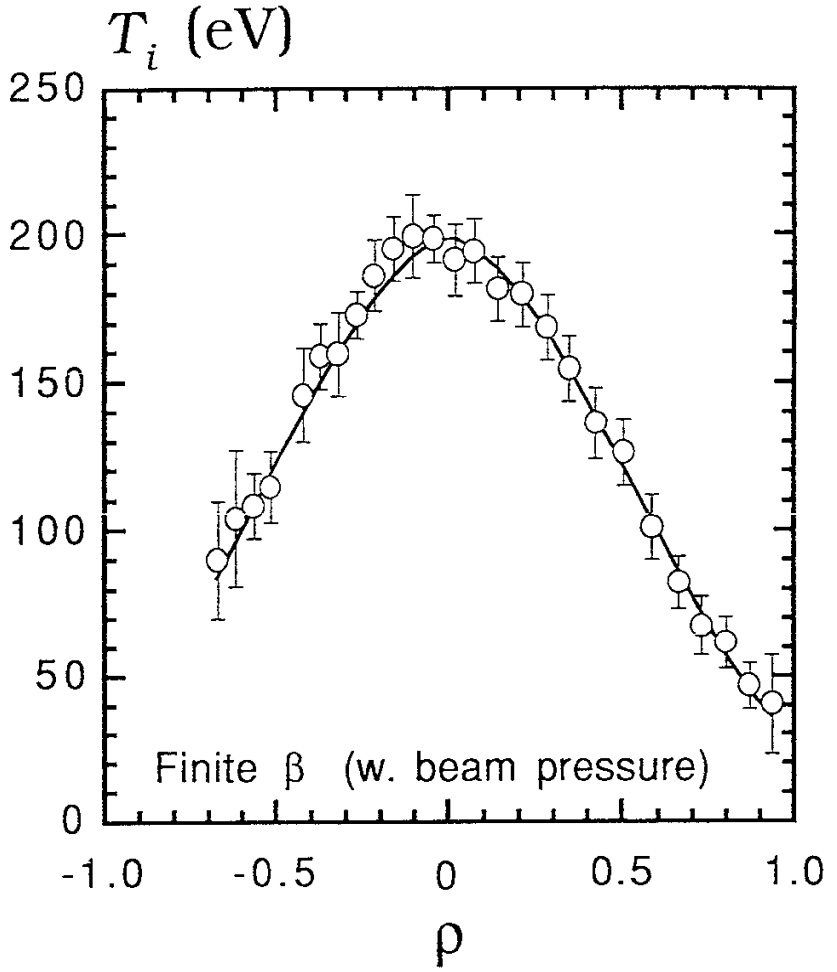

Figure 3 (b)

"Shafranov Shift in Low-Aspect-Ratio Heliotron/Torsatron CHS" by H.Yamada et al., *National Institute for Fusion Science, Nagoya 464-01, JAPAN*

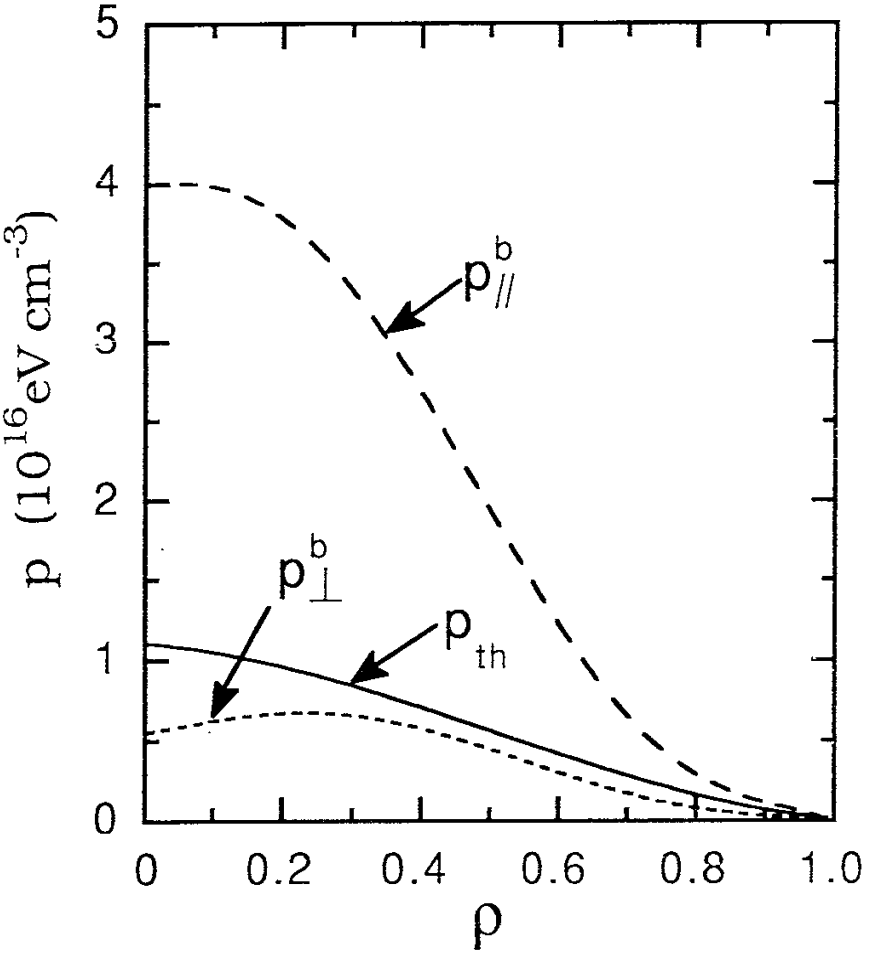

Figure 4

"Shafranov Shift in Low-Aspect-Ratio Heliotron/Torsatron CHS" by H.Yamada et al., *National Institute for Fusion Science, Nagoya 464-01, JAPAN*

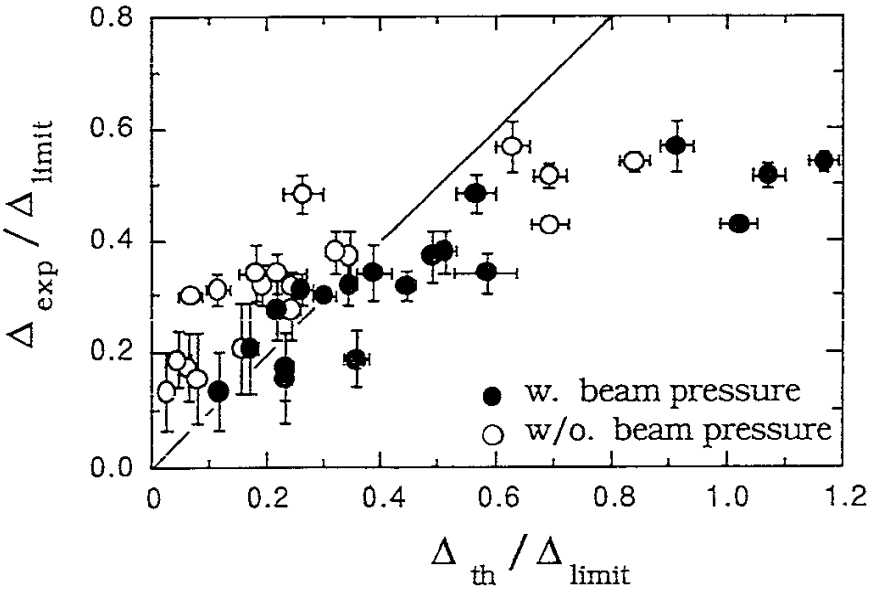

Figure 5

"Shafranov Shift in Low-Aspect-Ratio Heliotron/Torsatron CHS" by H.Yamada et al., *National Institute for Fusion Science, Nagoya 464-01, JAPAN*

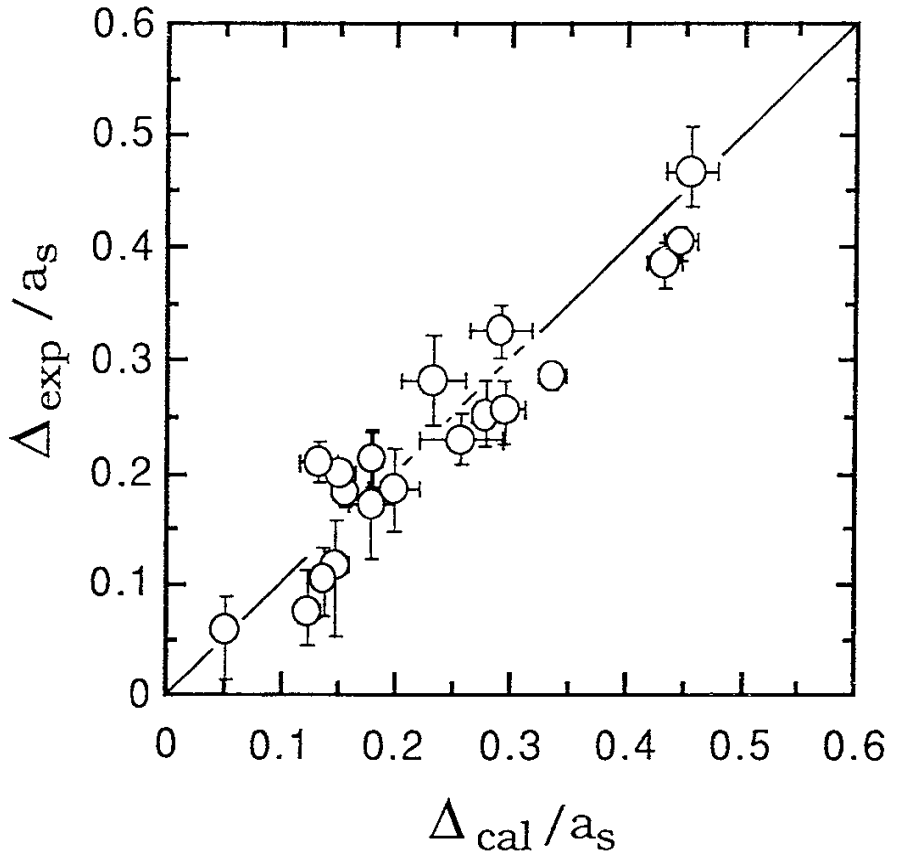

Figure 6

"Shafranov Shift in Low-Aspect-Ratio Heliotron/Torsatron CHS" by H.Yamada et al., *National Institute for Fusion Science, Nagoya 464-01, JAPAN*

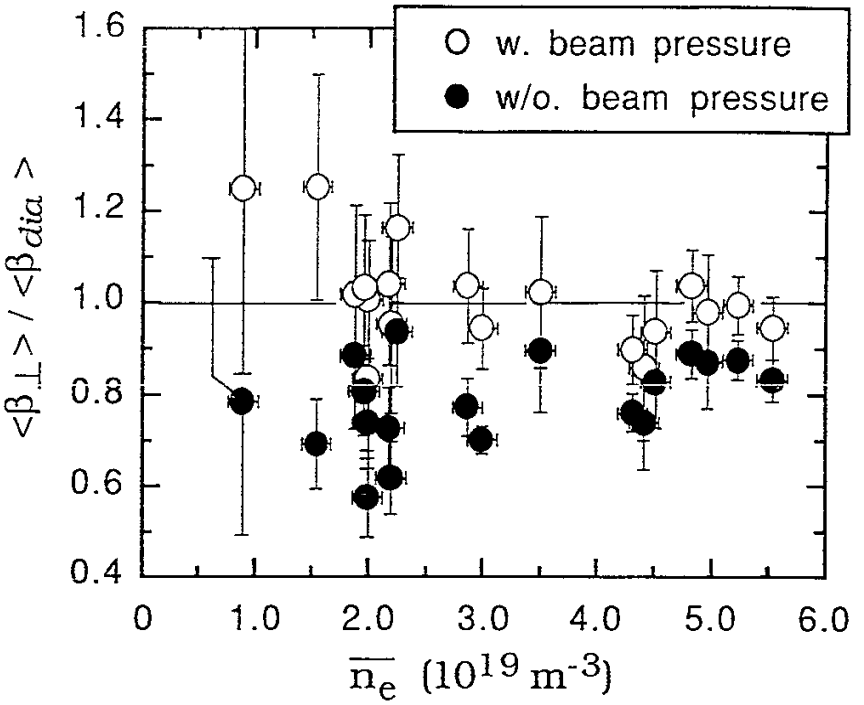

Figure 7

"Shafranov Shift in Low-Aspect-Ratio Heliotron/Torsatron CHS" by H.Yamada et al., *National Institute for Fusion Science, Nagoya 464-01, JAPAN*

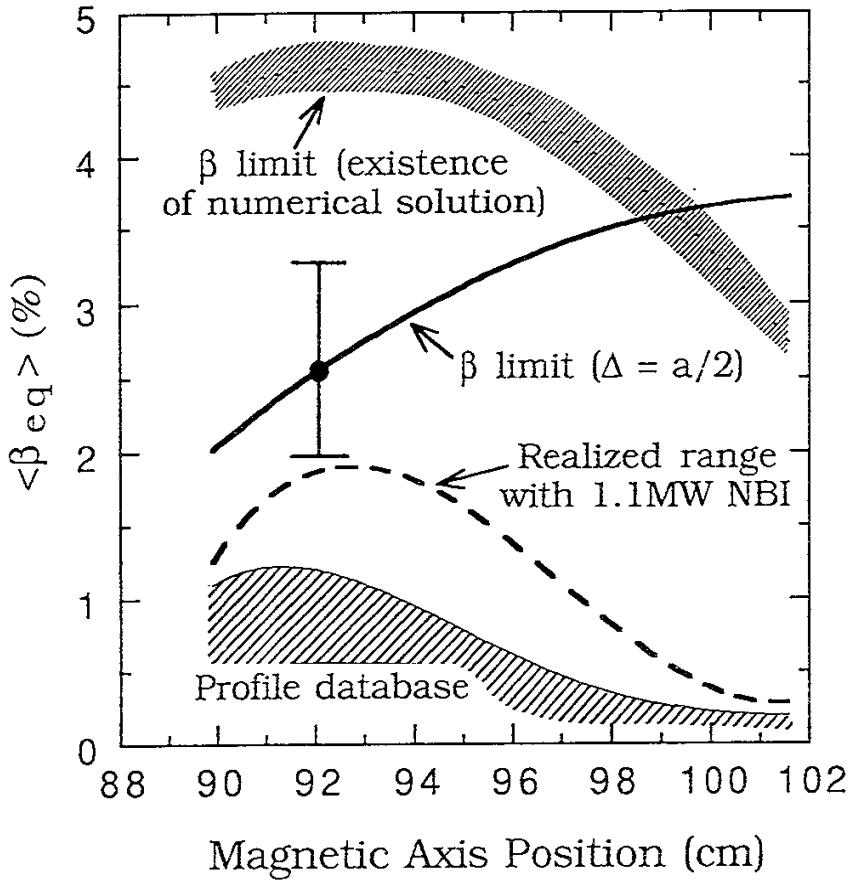

Figure 8

"Shafranov Shift in Low-Aspect-Ratio Heliotron/Torsatron CHS" by H.Yamada et al., *National Institute for Fusion Science, Nagoya 464-01, JAPAN*

Recent Issues of NIFS Series

NIFS-50 S.Koide, *3-Dimensional Simulation of Dynamo Effect of Reversed Field Pinch*; Sep. 1990

NIFS-51 O.Motojima, K. Akaishi, M.Asao, K.Fujii, J.Fujita, T.Hino, Y.Hamada, H.Kaneko, S.Kitagawa, Y.Kubota, T.Kuroda, T.Mito, S.Morimoto, N.Noda, Y.Ogawa, I.Ohtake, N.Ohyabu, A.Sagara, T. Satow, K.Takahata, M.Takeo, S.Tanahashi, T.Tsuzuki, S.Yamada, J.Yamamoto, K.Yamazaki, N.Yanagi, H.Yonezu, M.Fujiwara, A.Iiyoshi and LHD Design Group, *Engineering Design Study of Superconducting Large Helical Device*; Sep. 1990

NIFS-52 T.Sato, R.Horiuchi, K. Watanabe, T. Hayashi and K.Kusano, *Self-Organizing Magnetohydrodynamic Plasma*; Sep. 1990

NIFS-53 M.Okamoto and N.Nakajima, *Bootstrap Currents in Stellarators and Tokamaks*; Sep. 1990

NIFS-54 K.Itoh and S.-I.Itoh, *Peaked-Density Profile Mode and Improved Confinement in Helical Systems*; Oct. 1990

NIFS-55 Y.Ueda, T.Enomoto and H.B.Stewart, *Chaotic Transients and Fractal Structures Governing Coupled Swing Dynamics*; Oct. 1990

NIFS-56 H.B.Stewart and Y.Ueda, *Catastrophes with Indeterminate Outcome*; Oct. 1990

NIFS-57 S.-I.Itoh, H.Maeda and Y.Miura, *Improved Modes and the Evaluation of Confinement Improvement*; Oct. 1990

NIFS-58 H.Maeda and S.-I.Itoh, *The Significance of Medium- or Small-size Devices in Fusion Research*; Oct. 1990

NIFS-59 A.Fukuyama, S.-I.Itoh, K.Itoh, K.Hamamatsu, V.S.Chan, S.C.Chiu, R.L.Miller and T.Ohkawa, *Nonresonant Current Drive by RF Helicity Injection*; Oct. 1990

NIFS-60 K.Ida, H.Yamada, H.Iguchi, S.Hidekuma, H.Sanuki, K.Yamazaki and CHS Group, *Electric Field Profile of CHS Heliotron/Torsatron Plasma with Tangential Neutral Beam Injection*; Oct. 1990

NIFS-61 T.Yabe and H.Hoshino, *Two- and Three-Dimensional Behavior of Rayleigh-Taylor and Kelvin-Helmholz Instabilities*; Oct. 1990

NIFS-62 H.B. Stewart, *Application of Fixed Point Theory to Chaotic Attractors of Forced Oscillators;* Nov. 1990

NIFS-63 K.Konn., M.Mituhashi, Yoshi H.Ichikawa,*Soliton on Thin Vortex Filament;* Dec. 1990

NIFS-64 K.Itoh, S.-I.Itoh and A.Fukuyama,*Impact of Improved Confinement on Fusion Research;* Dec. 1990

NIFS -65 A.Fukuyama, S.-I.Itoh and K. Itoh,*A Consistency Analysis on the Tokamak Reactor Plasmas;* Dec. 1990

NIFS-66 K.Itoh, H. Sanuki, S.-I. Itoh and K. Tani,*Effect of Radial Electric Field on α-Particle Loss in Tokamaks;* Dec. 1990

NIFS-67 K.Sato,and F.Miyawaki,*Effects of a Nonuniform Open Magnetic Field on the Plasma Presheath*; Jan.1991

NIFS-68 K.Itoh and S.-I.Itoh,*On Relation between Local Transport Coefficient and Global Confinement Scaling Law;* Jan. 1991

NIFS-69 T.Kato, K.Masai, T.Fujimoto,F.Koike, E.Källne, E.S.Marmar and J.E.Rice,*He-like Spectra Through Charge Exchange Processes in Tokamak Plasmas;* Jan.1991

NIFS-70 K. Ida, H. Yamada, H. Iguchi, K. Itoh and CHS Group, *Observation of Parallel Viscosity in the CHS Heliotron/Torsatron* ; Jan.1991

NIFS-71 H. Kaneko, *Spectral Analysis of the Heliotron Field with the Toroidal Harmonic Function in a Study of the Structure of Built-in Divertor* ; Jan. 1991

NIFS-72 S. -I. Itoh, H. Sanuki and K. Itoh, *Effect of Electric Field Inhomogeneities on Drift Wave Instabilities and Anomalous Transport* ; Jan. 1991

NIFS-73 Y.Nomura, Yoshi.H.Ichikawa and W.Horton, *Stabilities of Regular Motion in the Relativistic Standard Map*; Feb. 1991

NIFS-74 T.Yamagishi, *Electrostatic Drift Mode in Toroidal Plasma with Minority Energetic Particles,* Feb. 1991

NIFS-75 T.Yamagishi, *Effect of Energetic Particle Distribution on Bounce Resonance Excitation of the Ideal Ballooning Mode,* Feb. 1991

NIFS-76 T.Hayashi, A.Tadei, N.Ohyabu and T.Sato, *Suppression of Magnetic Surface Breading by Simple Extra Coils in Finite Beta Equilibrium of Helical System;* Feb. 1991

NIFS-77 N. Ohyabu, *High Temperature Divertor Plasma Operation*; Feb. 1991

NIFS-78 K.Kusano, T. Tamano and T. Sato, *Simulation Study of Toroidal Phase-Locking Mechanism in Reversed-Field Pinch Plasma*; Feb. 1991

NIFS-79 K. Nagasaki, K. Itoh and S. -I. Itoh, *Model of Divertor Biasing and Control of Scrape-off Layer and Divertor Plasmas*; Feb. 1991

NIFS-80 K. Nagasaki and K. Itoh, *Decay Process of a Magnetic Island by Forced Reconnection*; Mar. 1991

NIFS-81 K. Takahata, N. Yanagi, T. Mito, J. Yamamoto, O.Motojima and LHDDesign Group, K. Nakamoto, S. Mizukami, K. Kitamura, Y. Wachi, H. Shinohara, K. Yamamoto, M. Shibui, T. Uchida and K. Nakayama, *Design and Fabrication of Forced-Flow Coils as R&D Program for Large Helical Device*; Mar. 1991

NIFS-82 T. Aoki and T. Yabe, *Multi-dimensional Cubic Interpolation for ICF Hydrodynamics Simulation*; Apr. 1991

NIFS-83 K. Ida, S.-I. Itoh, K. Itoh, S. Hidekuma, Y. Miura, H. Kawashima, M. Mori, T. Matsuda, N. Suzuki, H. Tamai, T.Yamauchi and JFT-2M Group, *Density Peaking in the JFT-2M Tokamak Plasma with Counter Neutral Beam Injection* ; May 1991

NIFS-84 A. Iiyoshi, *Development of the Stellarator/Heliotron Research*; May 1991

NIFS-85 Y. Okabe, M. Sasao, H. Yamaoka, M. Wada and J. Fujita, *Dependence of Au^- Production upon the Target Work Function in a Plasma-Sputter-Type Negative Ion Source;* May 1991

NIFS-86 N. Nakajima and M. Okamoto, *Geometrical Effects of the Magnetic Field on the Neoclassical Flow, Current and Rotation in General Toroidal Systems*; May 1991

NIFS-87 S. -I. Itoh, K. Itoh, A. Fukuyama, Y. Miura and JFT-2M Group, *ELMy-H mode as Limit Cycle and Chaotic Oscillations in Tokamak Plasmas;* May 1991

NIFS-88 N.Matsunami and K.Kitoh, *High Resolution Spectroscopy of H^+ Energy Loss in Thin Carbon Film;* May 1991

NIFS-89 H. Sugama, N. Nakajima and M.Wakatani, *Nonlinear Behavior of Multiple-Helicity Resistive Interchange Modes near Marginally Stable States;* May 1991

NIFS-90 H. Hojo and T.Hatori, *Radial Transport Induced by Rotating RF Fields and Breakdown of Intrinsic Ambipolarity in a Magnetic Mirror*; May 1991

NIFS-91 M. Tanaka, S. Murakami, H. Takamaru and T.Sato, *Macroscale Implicit, Electromagnetic Particle Simulation of Inhomogeneous and Magnetized Plasmas in Multi-Dimensions;* May 1991

NIFS-92 S. - I. Itoh, *H-mode Physics, -Experimental Observations and Model Theories-, Lecture Notes, Spring College on Plasma Physics, May 27 - June 21 1991 at International Centre for Theoretical Physics (IAEA UNESCO) Trieste, Italy ;* Jun. 1991

NIFS-93 Y. Miura, K. Itoh, S. - I. Itoh, T. Takizuka, H. Tamai, T. Matsuda, N. Suzuki, M. Mori, H. Maeda and O. Kardaun, *Geometric Dependence of the Scaling Law on the Energy Confinement Time in H-mode Discharges;* Jun. 1991

NIFS-94 H. Sanuki, K. Itoh, K. Ida and S. - I. Itoh, *On Radial Electric Field Structure in CHS Torsatron / Heliotron;* Jun. 1991

NIFS-95 K. Itoh, H. Sanuki and S. - I. Itoh, *Influence of Fast Ion Loss on Radial Electric Field in Wendelstein VII-A Stellarator;* Jun. 1991

NIFS-96 S. - I. Itoh, K. Itoh, A. Fukuyama, *ELMy-H mode as Limit Cycle and Chaotic Oscillations in Tokamak Plasmas;* Jun. 1991

NIFS-97 K. Itoh, S. - I. Itoh, H. Sanuki, A. Fukuyama, *An H-mode-Like Bifurcation in Core Plasma of Stellarators;* Jun. 1991

NIFS-98 H. Hojo, T. Watanabe, M. Inutake, M. Ichimura and S. Miyoshi, *Axial Pressure Profile Effects on Flute Interchange Stability in the Tandem Mirror GAMMA 10;* Jun. 1991

NIFS-99 A. Usadi, A. Kageyama, K. Watanabe and T. Sato, *A Global Simulation of the Magnetosphere with a Long Tail : Southward and Northward IMF;* Jun. 1991

NIFS-100 H. Hojo, T. Ogawa and M. Kono, *Fluid Description of Ponderomotive Force Compatible with the Kinetic One in a Warm Plasma* ; July 1991

NIFS-101 H. Momota, A. Ishida, Y. Kohzaki, G. H. Miley, S. Ohi, M. Ohnishi K. Yoshikawa, K. Sato, L. C. Steinhauer, Y. Tomita and M. Tuszewski *Conceptual Design of D-^{3}He FRC Reactor "ARTEMIS"* ; July 1991

NIFS-102 N. Nakajima and M. Okamoto, *Rotations of Bulk Ions and Impurities in Non-Axisymmetric Toroidal Systems* ; July 1991

NIFS-103 A. J. Lichtenberg, K. Itoh, S. - I. Itoh and A. Fukuyama, *The Role of Stochasticity in Sawtooth Oscillation* ; Aug. 1991

NIFS-104 K. Yamazaki and T. Amano, *Plasma Transport Simulation Modeling for Helical Confinement Systems;* Aug. 1991

NIFS-105 T. Sato, T. Hayashi, K. Watanabe, R. Horiuchi, M. Tanaka, N. Sawairi and K. Kusano, *Role of Compressibility on Driven Magnetic Reconnection ;* Aug. 1991

NIFS-106 Qian Wen - Jia, Duan Yun - Bo, Wang Rong - Long and H. Narumi, *Electron Impact Excitation of Positive Ions - Partial Wave Approach in Coulomb - Eikonal Approximation* ; Sep. 1991

NIFS-107 S. Murakami and T. Sato, *Macroscale Particle Simulation of Externally Driven Magnetic Reconnection;* Sep. 1991

NIFS-108 Y. Ogawa, T. Amano, N. Nakajima, Y. Ohyabu, K. Yamazaki, S. P. Hirshman, W. I. van Rij and K. C. Shaing, *Neoclassical Transport Analysis in the Banana Regime on Large Helical Device (LHD) with the DKES Code;* Sep. 1991

NIFS-109 Y. Kondoh, *Thought Analysis on Relaxation and General Principle to Find Relaxed State;* Sep. 1991